ECS Transactions, 41 (2) 147-155 (2011)
10.1149/1.3633663 ©The Electrochemical Society

Indium Oxide ALD using Cyclopentadienyl Indium and Mixtures of H_2O and O_2

J. W. Elam, J. A. Libera, and J. N. Hryn

Argonne National Laboratory, Argonne, Illinois 60439

This study describes how In_2O_3 films can be prepared by ALD using alternating exposures to cyclopentadienyl indium (InCp) and *combinations* of H_2O and O_2, even though H_2O and O_2 are ineffective when used individually. When H_2O and O_2 are used together, either as a simultaneous exposure or in the sequence H_2O-O_2 or O_2-H_2O, very uniform, highly conducting In_2O_3 films are deposited at 1.0-1.6 Å/cycle over large areas (12"x18") at temperatures as low as 100°C. In agreement with our published mechanism, in-situ Fourier transform infrared measurements revealed that the H_2O and O_2 work synergistically to facilitate the In_2O_3 ALD. Ex-situ measurements on films prepared over the deposition temperature range 100-250°C identified a remarkable correlation between the film structure and electrical properties around an amorphous-to-crystalline phase transition near 140°C.

Introduction

Nanostructured solar cells offer the promise of low cost photovoltaics to replace fossil fuels as our primary source of electricity. These devices utilize thin layers arranged in a folded geometry to achieve simultaneously a long optical path for complete solar absorption with a short diffusion path for the efficient collection of photogenerated charge carriers (1). In this way, acceptable power efficiencies can be realized without the need for expensive, high purity, highly crystalline materials. Atomic layer deposition (ALD) is an ideal technology for fabricating nanostructured solar cells because it yields precise, conformal coatings on high aspect ratio templates which are needed for building such devices (2,3). Consequently, we are developing ALD methods for depositing transparent conducting oxides (TCO) such as indium tin oxide (ITO) (4-6). ITO is one of the most widely used TCOs owing to its exceptional conductivity and transparency to visible light (7,8). Recently we synthesized nanostructured, dye-sensitized solar cells (DSSCs) using anodic aluminum oxide templates in which we conformally coated the inside of the high aspect ratio nanopores with ALD ITO and ALD TiO_2. We demonstrated that the ALD ITO layer increased the power efficiency of the DSSCs by a factor of 30x compared to devices prepared without the interdigitated ITO, thus demonstrating the tremendous advantage of radial charge collection in nanostructured solar cells (9).

The ITO process we employed for these previous studies utilized alternating exposures to cyclopentadienyl indium (InCp) and ozone (O_3) for the In_2O_3 ALD (4). Although both indium trichloride ($InCl_3$) and trimethyl indium (TMIn) have been used previously for In_2O_3 ALD, InCp was selected because $InCl_3$ will etch the In_2O_3 during the long exposures needed to infiltrate porous substrates (10), and TMIn does not show self-limited growth (11). During these studies we observed that the In_2O_3 was an effective O_3 destruction catalyst which meant that the In_2O_3 could decompose the O_3

precursor necessary to deposit the films, and this lead to non-uniform thickness profiles with thinner films deposited downstream in our viscous flow ALD reactor (12). Despite this shortcoming, we successfully infiltrated high aspect ratio nanopores with sufficient conformality to fabricate devices and this encouraged us to attempt scaling up the InCp/O_3 process to larger substrate areas. Unfortunately, the films had unacceptably large thickness non-uniformities when we prepared ALD In_2O_3 films on 18"x12" substrates (Fig. 6a), and this motivated us to search for an alternative process that did not require O_3. Although we had previously failed to deposit ALD In_2O_3 films using a number of oxygen sources (H_2O, O_2, H_2O_2, and N_2O) individually with InCp (4), we were surprised to discover that when H_2O and O_2 were used together, very uniform, In_2O_3 films were deposited over large areas (13).

In this manuscript we describe measurements made on In_2O_3 films deposited using InCp and combinations of H_2O and O_2 on fused silica and silicon substrates to deduce the relationships between the structure and properties of the ALD In_2O_3. In addition, we discuss in-situ Fourier transform infrared (FTIR) measurements performed to understand the growth mechanism. Finally, we show that this process is suitable for depositing In_2O_3 films on large area substrates.

Experimental

Indium oxide films were deposited using a custom ALD viscous flow reactor with a 5 cm ID flow tube (14). Ultrahigh purity nitrogen carrier gas (Airgas, 99.998%) continuously flowed through the reactor at 360 sccm and a pressure of 1.1 Torr. Cyclopentadienyl indium (InCp, Strem, 99.999%+ electronic grade) was held in a stainless steel bubbler heated to 40-45^{o}C and 90 sccm of the N_2 carrier gas was diverted through the bubbler during the InCp exposures. Ultrahigh purity oxygen (Airgas 99.995%) flowing at 200 sccm and water vapor from the head space of a deionized water reservoir were used as oxygen sources for the In_2O_3 ALD. The large area coating experiments utilized a custom cross-flow reactor installed in place of the 5 cm ID flow tube. The large area reactor could accommodate planar substrates with dimensions up to 12"x18"(13).

In-situ Fourier transform infrared (FTIR) measurements were made during the In_2O_3 ALD using a Nicolet 6700 with a liquid nitrogen-cooled MCT-B detector. For these measurements, the FTIR beam was diverted through CsI windows and into the ALD reactor. The windows were protected by gate valves which were closed during the ALD exposures to prevent deposition on the windows. The FTIR beam was directed through a sample comprised of ZrO_2 nanopowder pressed into a stainless steel grid to enhance the surface area of the sample and boost the absorption (15). Prior to the In_2O_3 ALD, the ZrO_2 powder was coated using 10 cycles of trimethyl aluminum (TMA, Aldrich, 97%) and deionized water for Al_2O_3 ALD.

Conventional metal oxide ALD consists of alternating exposures to a metal precursor, A, and a single oxygen source, B, so that one ALD cycle can be written: A/B. In this study In_2O_3 ALD was performed using combinations of two oxygen sources: oxygen (B1) and water (B2). The In_2O_3 ALD cycles were performed in three ways: simultaneous exposure (SE), A/(B1+B2); oxygen followed by water (OW), A/B1/B2; and water followed by oxygen (WO), A/B2/B1. For comparison, some films were prepared using just water or oxygen. The InCp exposure times were 3 s and the water and oxygen exposure times were 4 s. Purge times of 5 s were used between each exposure. These exposure times were determined to be saturating and the purge times were found to be

adequate based on in-situ quartz crystal microbalance (QCM) measurements performed at 175°C.

In_2O_3 films were deposited on Si(100) and fused silica substrates using 300 ALD cycles yielding films of 30-48 nm in thickness. To facilitate prompt and consistent nucleation of the ALD In_2O_3 films, the substrates were first coated with ~2 nm ALD Al_2O_3 using 20 cycles of TMA and deionized water with 2 s exposures and 5 s purge periods. Film thicknesses were determined using spectroscopic ellipsometry (J.A.Woolam Co. Alpha-SE). Ultraviolet-visible (UV-Vis) optical absorption measurements utilized a Cary-5000 spectrophotometer. X-ray diffraction (XRD) measurements were made on a Rigaku Miniflex Plus diffractometer using Cu Kα x-rays. The resistivity, carrier mobility, and carrier concentration were measured from films prepared on fused silica substrates with an Ecopia HMS-3000 Hall effect system.

Results and Discussion

Growth and Properties of In_2O_3 Films

Figure 1 shows the In_2O_3 ALD growth rates determined by spectroscopic ellipsometry for films prepared using 300 cycles of InCp and various oxygen sources at a deposition temperature of 200C. The growth rates for In_2O_3 films prepared using either

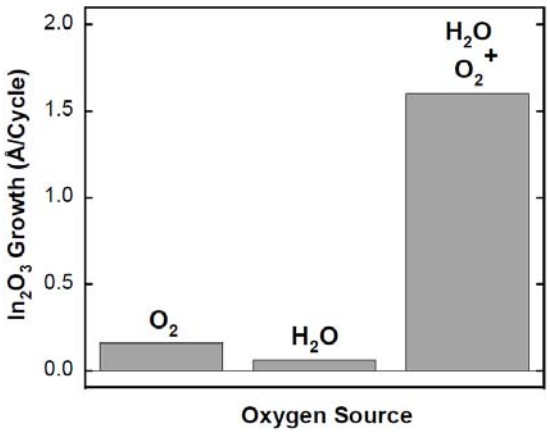

Figure 1: ALD In_2O_3 growth rates using InCp and various oxygen sources.

just O_2 or just H_2O were negligible (0.16 Å/cycle and 0.06 Å/cycle, respectively). In contrast, when O_2 and H_2O were used in a simultaneous exposure (SE), the ALD In_2O_3 growth rate was much higher at 1.6 Å/cycle.

The solid circles in Fig. 2 show growth rates for ALD In_2O_3 films prepared using the SE mode over the deposition temperature range 100-250°C. Over this temperature range the growth rate remained relatively high at over 1.0 Å /cycle. The gradual decrease in growth rate below 130°C is probably due to incomplete saturation because of slower reaction kinetics. We observed similar growth rate behavior using the OW and WO modes. The low temperature In_2O_3 growth is quite remarkable given that the previous InCp/O_3 process could not deposit ALD In_2O_3 films below 200°C (4). We performed XRD measurements for all of these films prepared on fused silica substrates and found that for growth temperatures below ~125°C the films were amorphous but above ~140°C the films were crystalline. The amorphous to crystalline transition temperature of ~140°C is indicated by the dashed line on Fig. 2.

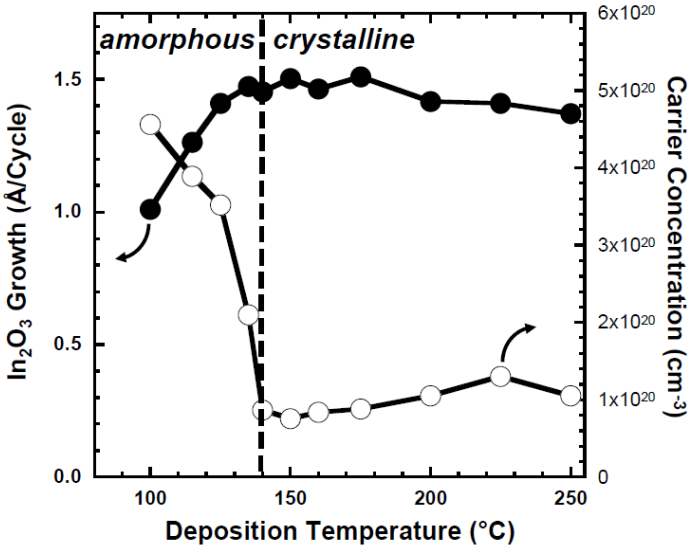

Figure 2: ALD In_2O_3 growth rate (solid symbols) and carrier concentration (open symbols) versus deposition temperature. Dashed line designates the amorphous to crystalline transition temperature as determined by X-ray diffraction.

Next we performed Hall probe measurements on the ALD In_2O_3 films deposited on fused silica over the full range of deposition temperatures. These measurements revealed that the ALD In_2O_3 films are highly conducting, with resistivity values in the range of 0.4-3.0x10^{-3} Ωcm. The most highly conducting films were the amorphous In_2O_3 films deposited using the SE mode with resistivities of 4.0x10^{-4} Ωcm. The electrical characteristics for the ALD In_2O_3 films exhibited an interesting dependence on the deposition temperature. For instance, Fig. 2 shows the carrier concentration values deduced from the Hall probe measurements. At the lowest deposition temperature of 100°C, the carrier concentration was quite high at 4.6x10^{20} cm^{-3}. The carrier concentration decreased abruptly near the amorphous to crystalline transition temperature and settled to a nearly constant value of ~1x10^{20} cm^{-3} between 140-250°C. Likewise, the mobility (not shown) increased abruptly at the transition temperature and remained relatively high at 60-110 cm/Vs for the higher deposition temperatures. Our interpretation of these results is that at the lower growth temperatures where the In_2O_3 films are amorphous, the carrier concentration is high due to the greater number of defects in the films such as oxygen vacancies that donate charge carriers. Similarly, the mobility is low as a result of scattering from these defect sites. The mobility is greater for the crystalline In_2O_3 films deposited at higher temperatures because of the more effective charge transport through the well-ordered In_2O_3 crystals. Likewise, the carrier concentration is lower because the crystalline films are less defective and poses fewer oxygen vacancies.

Mechanism for In_2O_3 ALD

In our previous study of In_2O_3 ALD using combinations of H_2O and O_2 we performed in-situ quartz crystal microbalance (QCM) and quadrupole mass spectrometry (QMS) measurements to investigate the mechanism for In_2O_3 ALD (13). These measurements revealed that regardless of the deposition mode (SE, OW, or WO), there was always a release of cyclopentadiene (HCp) during the H_2O exposures, and the O_2

exposures always increased the mass of the film without producing any gaseous products. Based on these and other observations, we postulated the mechanism for In_2O_3 ALD

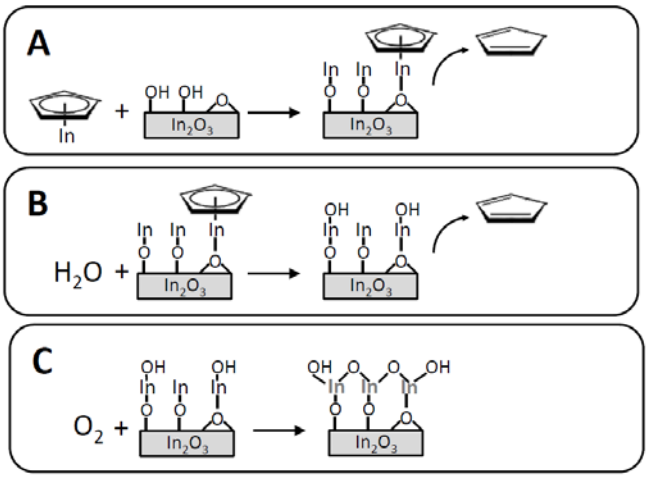

Figure 3: Schematic depiction of the mechanism for In_2O_3 ALD. In step **A**, InCp reacts with hydroxyl groups and surface oxygen releasing most of the Cp ligands as HCp. In step **B**, H_2O liberates the remaining Cp from the surface and repopulates the surface with hydoxyl groups but the In remains in a reduced state (e.g. +1). In step **C**, O_2 adsorbs on the surface without releasing any product and oxidizes the In to the +3 oxidation state.

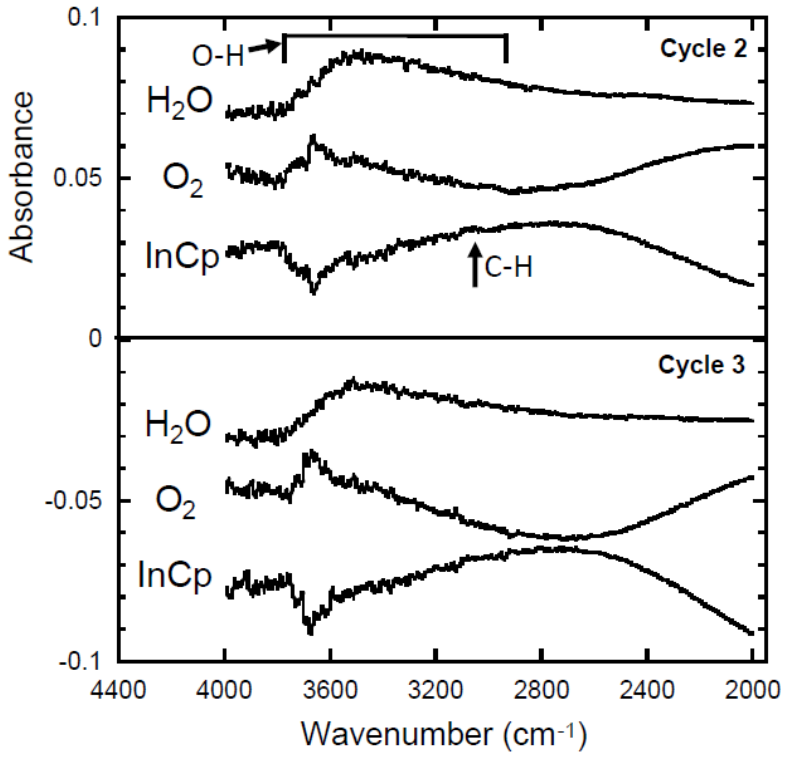

Figure 4: In situ FTIR spectra recorded during the second and third ALD In_2O_3 cycles on an Al_2O_3 surface. The spectral region for the O-H stretch and the anticipated location of the C-H stretch are indicated in the top panel.

depicted in Fig. 3. In step **A**, InCp reacts with hydroxyl groups and surface oxygen releasing most of the Cp ligands as HCp. In step **B**, H_2O liberates the remaining Cp and repopulates the surface with hydoxyl groups but the indium remains in a reduced state (e.g. +1). In step **C**, O_2 adsorbs on the surface without releasing any gaseous product and oxidizes the indium to the +3 oxidation state.

In the present study, we performed in-situ Fourier transform infrared transmission (FTIR) measurements to further evaluate the mechanism for In_2O_3 ALD and in particular to identify the surface functional groups and to observe changes in the indium oxidation state. The top panel of Fig. 4 shows FTIR spectra recorded following the H_2O and O_2 exposures of the second In_2O_3 cycle on an ALD Al_2O_3 surface. Both of these spectra are referenced to the previous InCp exposure. The broad peak between 2800-3800 cm^{-1} after the H_2O exposure results from hydroxyl (OH) groups on the In_2O_3 surface (11). These hydroxyl groups persist after the subsequent O_2 exposure. The spectrum labeled InCp on the top panel shows the FTIR spectrum after the following InCp exposure referenced to the preceding O_2 spectrum, and demonstrates that the hydroxyls are consumed during the InCp exposure. We failed to see the expected feature at ~3100 cm^{-1} corresponding to the C-H stretches of the Cp ligand following the InCp exposures (16). However, this feature is likely to be below our detection limit since the Cp coverage is only ~10% the OH coverage, and because the C-H stretch is typically ~1/10 the intensity of the corresponding O-H stretch. The bottom panel of Fig. 4 shows that the spectral pattern for hydroxyl formation and consumption is cyclic.

FTIR spectra were recorded following each precursor exposure for 10 In_2O_3 ALD cycles. Figure 5 plots the absorbance at 2000 cm^{-2} from these measurements. This

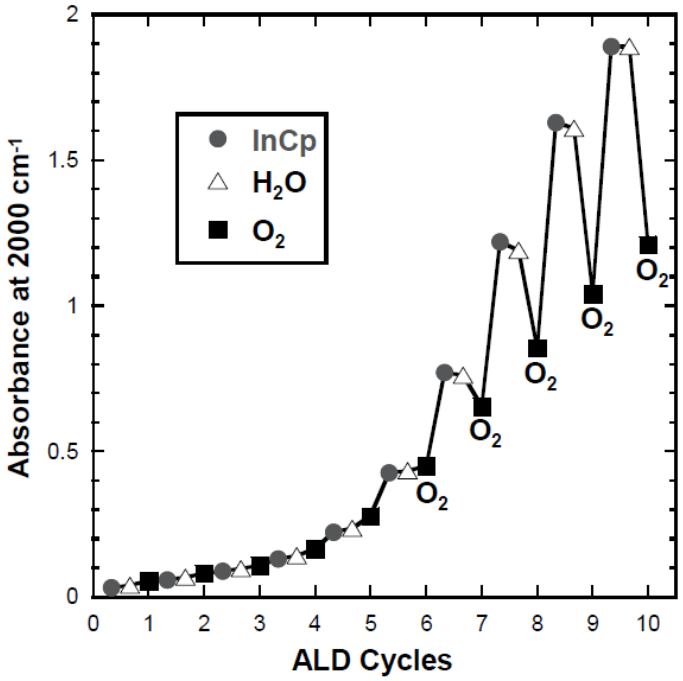

Figure 5: Intensity of absorbance at 2000 cm^{-2} determined from FTIR spectra acquired following each precursor exposure during In_2O_3 ALD on an ALD Al_2O_3 surface. The overall increase in absorbance reflects the nucleation and growth of the ALD In_2O_3. The decrease in absorbance following each O_2 exposure results from the decrease in carrier concentration that accompanies oxidation of the surface indium.

frequency was selected to quantify changes in the background absorbance because no surface functional groups absorb in this region. The overall envelope of the increasing absorbance reflects the nucleation and growth of the ALD In_2O_3 on the Al_2O_3 surface and

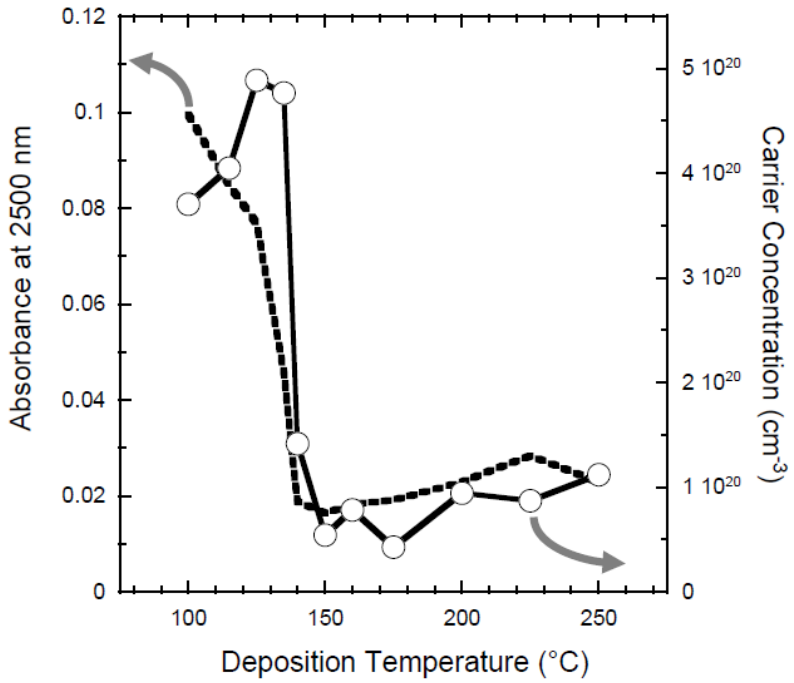

Figure 6: Transport properties of ALD In_2O_3 films prepared on fused silica substrates versus deposition temperature. Open circles: carrier concentration as determined using Hall probe measurements. Dashed line: optical absorbance at 2500 nm as determined from UV-Vis absorption measurements.

matches precisely the behavior observed by QCM. However, the detailed structure revealed in Fig. 5, and in particular the absorbance decreases that accompany each O_2 exposure, reflect changes in the indium oxidation state. According to Drude theory, the infrared background absorbance increases with the number of charge carriers in semiconducting samples (17). The increase in IR absorbance following the InCp exposures suggests that the indium deposits in a reduced state and contributes charge carriers. Evidently the indium remains reduced following the H_2O exposures because the absorbance does not change. Finally, the O_2 oxidizes the indium which removes the charge carriers so that the absorbance drops.

To assess this interpretation, we performed optical absorption measurements for a series of ALD In_2O_3 films prepared over the deposition temperature range 100-250°C. Figure 6 shows that the near-IR absorption of these films at 2500 nm is highest for the films prepared at the lowest temperatures but decreases abruptly at ~125°C and remains low for the films prepared at higher temperatures. This trend matches the trend in carrier concentrations versus deposition temperature measured for the same films (open circles in Fig. 6). This correlation between the IR absorbance and the carrier concentration in the ALD In_2O_3 strengthens our interpretation of Fig. 5. Taken together, the optical measurements confirm the model proposed in Fig. 3: surface hydroxyls mediate the Cp ligand release and O_2 serves the function of oxidizing the surface indium.

Scale-up of In_2O_3 ALD

One motivation for this study was to develop an alternative process for In_2O_3 ALD that did not require O_3. Figure 7a shows that when alternating cycles of InCp and O_3 were used to deposit ALD In_2O_3 on a 12"x18" substrate, the resulting films were extremely non-uniform with an average growth rate variation of ±45% and a maximum variation of 250%. The In_2O_3 films are thinner along the axial dimension downstream of the O_3 injection point and also laterally on either side of the main flow stream. We attribute this nonuniformity to thermal decomposition of the O_3 precursor which is

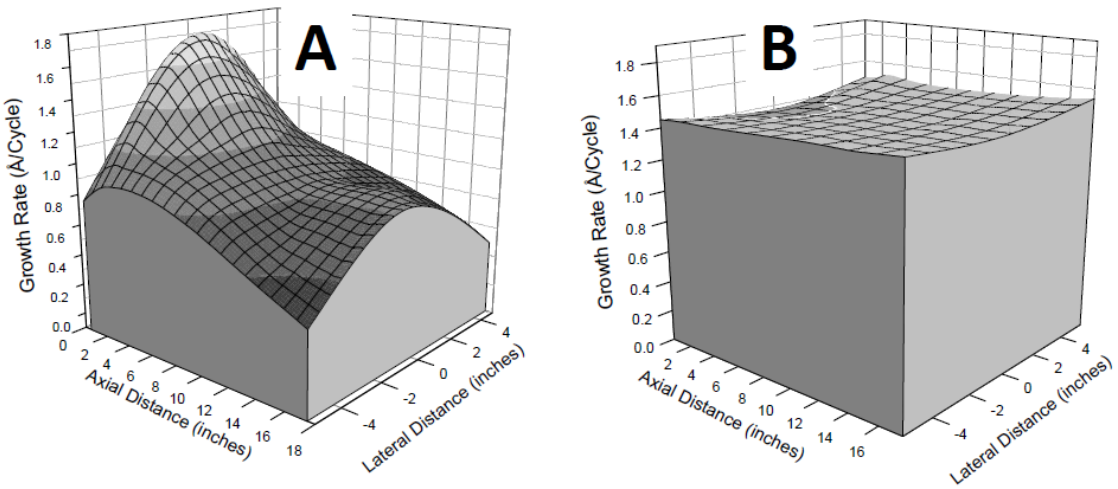

Figure 7: Spatial variation in ALD In_2O_3 growth rates determined from spectroscopic ellipsometry measurements performed on 12x18" substrates for films prepared using InCp/O_3 (A) and InCp/O_2/H2O using the OW mode (B).

catalyzed by the In_2O_3 surface because (4,12). In contrast, using simultaneous exposures to O_2 and H_2O in place of O_3, the growth rate uniformity is greatly improved (Fig. 7b). In this case, the average growth rate variation was only ±2%. We observed excellent uniformity in both the thickness and physical properties of the ALD In_2O_3 films prepared using the SE, OW, and WO growth modes and at all of the deposition temperatures studied in the range 100-250°C.

Conclusions

In conclusion, this study describes how ALD In_2O_3 films can be prepared using alternating exposures to cyclopentadienyl indium (InCp) and *combinations* of H_2O and O_2, even though H_2O and O_2 are ineffective when used individually. Ex-situ measurements on films prepared over the temperature range 100-250°C identified a remarkable correlation between the film structure and electrical properties around an amorphous-to-crystalline phase transition near the deposition temperature of 140°C. In-situ Fourier transform infrared measurements support the model we proposed earlier that the H_2O and O_2 work synergistically to facilitate the In_2O_3 ALD.

Acknowledgements

This work was supported by the U.S. Department of Energy, EERE-Solar Energy Technologies Program under FWP-4911A. The in-situ analysis was supported as part of the Argonne-Northwestern Solar Energy Research (ANSER) Center, an Energy Frontier Research Center funded by the U.S. Department of Energy, Office of Science, Office of Basic Energy Sciences under Award Number DE-SC0001059. Argonne is supported by the U. S. Department of Energy, Office of Science, Office of Basic Energy Sciences, under Contract No. DE-AC02-06CH11357 operated by UChicago Argonne, LLC.

References:

1 D. R. Rolison, R. W. Long, J. C. Lytle, A. E. Fischer, C. P. Rhodes, T. M. McEvoy, M. E. Bourga, and A. M. Lubers, *Chem. Soc. Rev.*, **38**, 1, 226, (2009).

2 M. Ritala and M. Leskela, 2001, "Atomic Layer Deposition", in *Handbook of Thin Film Materials*, edited by H. S. Nalwa (Academic Press, San Diego), Vol. 1, pp. 103.

3 S. M. George, *Chemical Reviews*, **110**, 1, 111, (2010).

4 J. W. Elam, A. B. F. Martinson, M. J. Pellin, and J. T. Hupp, *Chem. Mater.*, **18**, 15, 3571, (2006).

5 J. W. Elam, D. A. Baker, A. J. Hryn, A. B. F. Martinson, M. J. Pellin, and J. T. Hupp, *J. Vac. Sci. Tech. A*, **26**, 2, 244, (2008).

6 J. W. Elam, D. A. Baker, A. B. F. Martinson, M. J. Pellin, and J. T. Hupp, *J. Phys. Chem. C*, **112**, 6, 1938, (2008).

7 P. P. Edwards, A. Porch, M. O. Jones, D. V. Morgan, and R. M. Perks, *Dalton Trans.*, 19, 2995, (2004).

8 B. G. Lewis and D. C. Paine, *MRS Bull.*, **25**, 8, 22, (2000).

9 A. B. F. Martinson, J. W. Elam, J. Liu, M. J. Pellin, T. J. Marks, and J. T. Hupp, *Nano Letters*, **8**, 9, 2862, (2008).

10 T. Asikainen, M. Ritala, and M. Leskela, *J Electrochem Soc*, **141**, 11, 3210, (1994).

11 A. W. Ott, J. M. Johnson, J. W. Klaus, and S. M. George, *Appl. Surf. Sci.*, **112**, 205, (1997).

12 H. C. M. Knoops, J. W. Elam, J. A. Libera, and W. M. M. Kessels, *Chem. Mater.*, **23**, 9, 2381, (2011).

13 J. A. Libera, J. N. Hryn, and J. W. Elam, *Chem. Mater.*, **23**, 8, 2150, (2011).

14 J. W. Elam, M. D. Groner, and S. M. George, *Rev. Sci. Instrum.*, **73**, 8, 2981, (2002).

15 J. D. Ferguson, A. W. Weimer, and S. M. George, *J. Vac. Sci. Tech. A*, **23**, 1, 118, (2005).

16 M. Kroger-Laukkanen, M. Peussa, M. Leskela, and L. Niinisto, *Appl. Surf. Sci.*, **183**, 3-4, 290, (2001).

17 A. Gibson, *J. Sci. Instrum.*, **35**, 273, (1958).